Antibacterial Activity of Ordered Gold Nanorod Arrays

Yuejing Zhu,[†,‖] Mohankandhasamy Ramasamy,[†,‖] and Dong Kee Yi*[‡,§]

[†]Department of Bionanotechnology, Gachon University, Seongnam 461701, Republic of Korea
[‡]Department of Chemistry, Myongji University, Yongin 449-728, Republic of Korea
[§]Department of Energy and Biotechnology, Myongji University, Yongin 449-728, Republic of Korea

Ⓢ Supporting Information

ABSTRACT: Well-packed two- and three-dimensional (2D and 3D) gold nanorod (AuNR) arrays were fabricated using confined convective arraying techniques. The array density could be controlled by changing the concentration of the gold nanorods solution, the velocity of the moving substrate, and the environment air-temperature. The hydrophilic behavior of glass substrates before and after surface modification was studied through contact angle measurements. The affinity and alignment of the AuNR arrays with varying nanorod concentrations and the resulting different array densities were studied using field emission scanning electron microscopy (FE-SEM). Under stable laser intensity irradiation, the photothermal response of the prepared arrays was measured using a thermocouple and the results were analyzed quantitatively. Synthesized AuNR arrays were added to *Escherichia coli* (*E. coli*) suspensions and evaluated for photothermal bactericidal activity before and after laser irradiation. The results showed promising bactericidal effect. The severity of pathogen destruction was measured and quantified using fluorescence microscopy, bioatomic force microscopy (Bio-AFM) and flow cytometry techniques. These results indicated that the fabricated AuNR arrays at higher concentrations were highly capable of complete bacterial destruction by photothermal effect compared to the low concentration AuNR arrays. Subsequent laser irradiation of the AuNR arrays resulted in rapid photoheating with remarkable bactericidal activity, which could be used for water treatment to produce microbe-free water.

KEYWORDS: *gold nanorods, E. coli, gold nanorod arrays, convective assembly, photothermal*
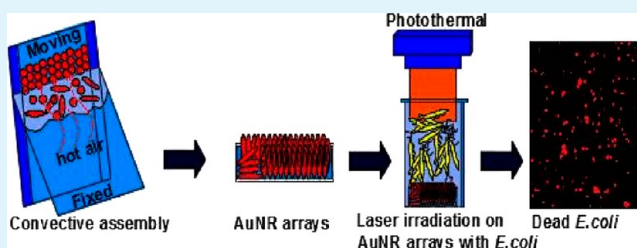
1. INTRODUCTION

Pathogenic bacterial infection through water consumption persists to be one of the most challenging problems today against healthy human life. Biologically diversified bacterial pathogens, which give rise to globally important diseases such as tuberculosis, pneumonia, and food borne illnesses, are the major threats we face today.[1,2] Among them, the Gram-negative bacterium *Escherichia coli* is a widespread one which causes serious food poisoning in humans.[3,4] Even though antibiotics are at the frontline of inhibition of bacterial infections, emerging antibiotic resistance in pathogens motivates research to produce highly efficient antimicrobial agents.[5,6] Therefore, a novel method for antibacterial therapy is needed, urgently.

Since ancient days to the recent decades the development of metal nanoparticles has received a great deal of attention in the fight against pathogenic bacteria.[7−9] Owing to the simple synthesis method, unique photophysical properties, and biocompatibility, Au nanoparticles have been applied in various biological fields. Due to surface plasmon resonance (SPR) properties, various forms of Au nanoparticles have been applied in heating, sensing, imaging, and drug delivery.[10−13] Furthermore, by changing their shape, the SPR frequency at which Au nanoparticles strongly absorb light energy can be tuned, when irradiated with near-infrared (NIR) laser light. The absorbed kinetic energy of the oscillated electrons is converted

into heat, subsequently generating high temperature in the surrounding environment.[14−16] Compared with other shapes, such as spherical nano gold particles, Au nanorods (AuNRs) can absorb and scatter laser light wavelengths in a wide range from the visible to the near-infrared region by changing the aspect ratio (length/width), which makes AuNRs superior candidates for photothermal bacterial lysis.[17,18]

Different techniques have been reported for the preparation of nanoparticle arrays for various applications.[19−22] In our study, confined convective nanoparticle arraying techniques driven by the principle of solvent evaporation have been adopted to produce uniform AuNR arrays. Previous research on photothermal bacteria lysis in water has focused on the activity of individual AuNRs, but AuNR arrays have not yet been tested for their photoheated bactericidal effect.[23,24] Herewith, for the first time, we propose a photothermal method of pathogenic bacteria destruction using AuNR arrays. Compared with dispersed AuNRs in solution, array-typed AuNRs can form 2D plate-shaped heating sources for typical applications, and has a potential in continuous and stable water purifying system.
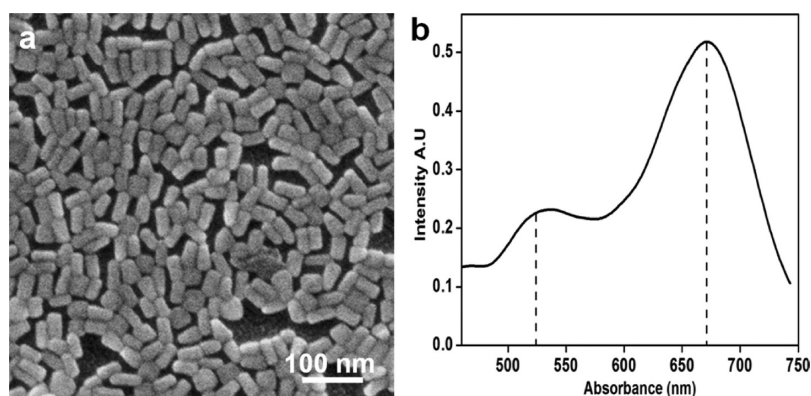
Figure 1. (a) FE-SEM micrograph of gold nanorods (AuNRs). (b) UV–vis spectrum of AuNRs with transverse peak at 520 nm and longitudinal peak at 670 nm.

In this study, the synthesis of well aligned AuNR arrays by a convective assembly method is reported for *E. coli* eradication. The severity of photothermal-based bacterial lysis of the resulting AuNR arrays is also reported, measured using different microscopy techniques. Expanding on previous reports that the photothermal effect can destroy the living cell,[9,25,26] our work is designed to utilize different densities of AuNR arrays for efficient pathogen destruction.

2. EXPERIMENTAL SECTION

2.1. Materials. The *E. coli* (KACC 10005) was obtained from the Korean Agriculture Collection Centre, Republic of Korea. Luria–Bertani (LB) broth was purchased from AMERSCO. Cetyltrimethyl-lammonium bromide (CTAB) was purchased from Alfa Aesar. 3-Mercaptopropyl trimethoxysilane (MPTMS), ammonium hydroxide (NH_4OH; 28 wt % in water), sodium borohydride ($NaBH_4$), silver nitrate ($AgNO_3$), ascorbic acid, hydrogen tetrachloroaurate(III) trihydrate ($HAuCl_4 \cdot 3H_2O$), ethanol, methanol, and sulfuric acid (H_2SO_4) were purchased from Sigma-Aldrich. Hydrogen peroxide (H_2O_2, Extra Pure) was purchased from Daejung Chemicals & Metals Co. Ltd., Republic of Korea.

2.2. Preparation of AuNRs. AuNRs were prepared by a modified seed-mediated method available elsewhere.[27,28] At first, the seed solution was prepared by mixing 250 μL of 0.01 M $HAuCl_4$ in 7.5 mL of 0.1 M CTAB and 600 μL of ice-cold 0.01 M $NaBH_4$ under vigorous stirring at room temperature. The growth solution was prepared by adding 400 μL of 0.01 M $HAuCl_4$, 64 μL of 0.1 M ascorbic acid and 35.6 μL of 0.1 M $AgNO_3$ into the 9.5 mL of 0.1 M CTAB. Finally, 10 μL of the 2.5 h old seed solution was added to the solution, and the mixture aged for 24 h at ambient temperature. Here, the silver nitrate allows the better shape control for AuNRs formation, whereas the ascorbic acid functions as a reducing agent.

2.3. Characterization of AuNRs. UV–visible-NIR spectrophotometer (Varian CARY 50, Varian, Inc.) was used to record the absorbance spectrum of the AuNRs solution. Shape, size, and the arrangements of AuNRs were studied using field emission scanning electron microscopy (FE-SEM) (JEOL Corp., JSM6700F).

2.4. Surface Derivatization of Substrate with Alkoxysilane. The glass slides were cleaned and modified using MPTMS solution followed by piranha treatment. Initially, the slides were sonicated in ethanol for 2 min to remove any surface contamination; then, they were treated under extreme caution with freshly made piranha solution (5 parts of 98% H_2SO_4 to 1 part 30% H_2O_2 at 60 °C) for 30 min to make oxygenated substrates. After they cooled to room temperature, the slides were rinsed successively with deionized water (DI water), followed by ethanol and methanol. Immediately, the slides were incubated in a methanolic MPTMS solution for 30 min. Prior to this, methanolic alkoxysilane solution had been prepared by mixing MPTMS and methanol with the volume ratio of 1:5, adjusting the pH to 4 using 1% sulfuric acid, and hydrolyzed by stirring for 2 h.

Afterward, the substrates were washed with methanol and water sequentially and sintered in a vacuum oven at 80 °C for 1 h.[29]

Caution! The Piranha solution is very aggressive; thus, proper care should be taken when in use.

Water contact-angle measurements were obtained on untreated, piranha-treated, and MPTMS-coated glass substrates in order to examine the hydrophobic properties of these three surfaces. Measurements were obtained at room temperature using an OCA-30 goniometer equipped with a microliter syringe (Future Digital Scientific Corp.). With a droplet of DI water, each sample was measured over 10 times, and the samples were photographed. The data was analyzed by Image XP 5.9.

2.5. Fabrication of AuNR Arrays. The aqueous AuNRs solutions were centrifuged and concentrated to 10, 20, and 33.3 mg/mL. The AuNRs were arrayed by the confined convective assembly technique.[30,31] The aqueous solution was dropped into the junction of the fixed glass slide and the moving glass substrate in the assembly. Subsequently, the back substrate was set to move at the rate of 20 μm/s while hot air was blown toward the interface of the substrates and the AuNRs solution. The fabricated AuNR arrays were imaged and quantified using FE-SEM.

2.6. Photothermal Energy Conversion of AuNR Arrays. The AuNR arrayed substrate was cut into appropriate sizes and immersed in DI water which was placed inside a sterilized tube. A calibrated red laser from the DPSS laser (Dream laser system, Japan) at the wavelength of 671 nm was used as the electron excitation source. The wavelength of exposure was closely matched with the longitudinal SPR band of the AuNRs. The light beam passed through the aperture was centered on the flat surface of the substrate. Previously, the intensity measurements had been made using a laser power meter, which was also used to stabilize the laser at 200 mW throughout the experiment. To measure the efficiency of photothermal energy conversion of our AuNR array substrates, the temperature increase was recorded by a thermocouple (K type, Omega) connected with a data acquisition system (34970, Agilent, Santa Clara, CA).

2.7. Antimicrobial Activity of AuNR Arrays upon Laser Irradiation. *E. coli* (KACC 10005) was cultured in LB broth at 37 °C for 18 h. The organisms were harvested by centrifugation, resuspended in saline, and adjusted to 10^8 cells/mL using spectrophotometer (OD_{600} of 0.1). At first, in a special custom-made tube, the AuNRs arrayed substrate was placed horizontally for the photothermal treatment. Then, the bacterial cell suspension was added on to it and subjected to continuous laser irradiation from a distance of up to 1 mm to attain a constant maximum temperature. This process was repeated for all the three different concentrations of AuNR arrayed substrates to analyze the photothermal impact on bacterial viability. After irradiation, the bacteria suspension was removed and stained using Live/Dead BacLight Bacterial Viability Kit (Invitrogen), as per manufacturer's protocol. The stained samples were analyzed using laser scanning fluorescence microscopy (Nikon Eclipse TE 2000-U)

and fluorescence-activated cell sorting (BD FACSCalibur) to measure the mortality rate of bacteria.

2.8. Impact of Direct Heat. The difference between the amount of heat produced over a certain interval of time by the photothermal method and that of the hot-plate-bath (Heidolph, MR Hei standard, 850 W) method was studied, while the thermal response of each method was plotted as a function of time. Subsequently, the antibacterial efficacy of direct heating on the bacterial suspensions was analyzed by using a bath heated for 20 min on a hot plate or via the photothermal method. The treated bacterial sample was mixed with the Live/Dead dye for the quantitative analysis of the number of cells killed by heat using a fluorescence microscope.

All experiments were carried out three times for each sample and the results were expressed as a mean ± standard deviation.

3. RESULTS AND DISCUSSION

3.1. Characterization of AuNRs. AuNRs with an aspect ratio of ≈2.5 were constructed in an aqueous solution using a cationic surfactant CTAB, via improved seed-mediated method. AuNRs were washed by multiple centrifugation processes to remove the dense layer of excess CTAB for reducing the toxicity.

The FE-SEM image in Figure 1a shows the consistent size of 19.78 ± 0.9 nm $\times$ 49.23 ± 2.1 nm for the produced AuNRs. The corresponding UV−vis spectrum of the AuNRs in Figure 1b illustrates the transverse localized surface plasmon resonance (LSPR) peak at 520 nm and a longitudinal LSPR peak at 670 nm.

3.2. Mechanism of Pretreatment in Surface Derivatization on Glass Substrates. The influence of surface modification of the glass substrate was quantified using contact angle measurements. Initially, the glass plates were cleaned and hydroxylated to make the glass substrate more hydrophilic. The glass substrates were further silanol derivatized with MPTMS. Here the MPTMS formed an adhesive layer with three-dimensional network structure on the substrate. It was produced via hydrolysis and condensation reactions after leaving the mercapto groups which oriented away from the substrate.[32,33] Figure 2a−c depicts the wetting property of
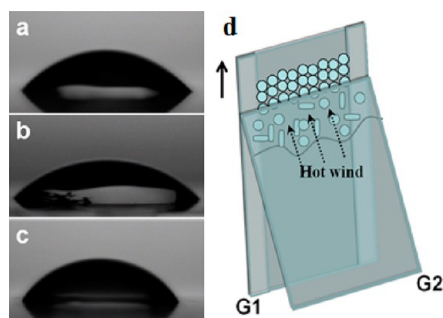

Figure 2. Profile of the water drop on the (a) untreated glass plate, (b) piranha treated glass plate, (c) MPTMS coated glass plate having contact angles of 52.43°, 24.49°, and 66.66°, respectively. (d) Schematic diagram of the confined convective assembly. G1 is the moving glass plate, and G2 is the fixed glass plate.

untreated and treated glass substrates which were measured under laboratory conditions. The contact angle for untreated glass slide was 52.43°. After piranha treatment, the contact angle decreased to 24.49°, yielding a hysteresis of 28.14°. The observed difference is attributed to the additional hydroxyl groups deposited on the glass surface by the piranha solution. Following by MPTMS activation, the contact angle increased to

66.66°, an observation in agreement with results previously reported in the literature.[34,35] The contact angle measurement can be used to quantify the wettability of the glass plate surface and analyze how it is altered by the addition of surface-modifying groups such as thiol and amine. An increased contact angle was observed for the MPTMS treated glass substrate rendering it satisfactory for the attachment materials containing specific chemical moieties of high affinity. As noted in the Experimental Section, the polar DI water droplet was formed on the sample plate 10 times and the contact angle was measured. The value of contact angle reported is the average of these 10 measurements.

3.3. Formation of AuNR Arrays with Different Densities of AuNRs Solutions. Figure 2d depicts the experimental setup showing the making of AuNR array using convective assembly technology. The moving vertical glass plate (G1) at a steady rate and the stable gradient glass plate (G2) were involved in the array formation. In between the two glass plates, there was a plate-suspension-air contact, where the successive AuNR arrays were formed. Array formation is controlled by three parameters: (1) capillary forces, (2) water evaporation, and (3) convective transfer.[36] After the introduction of the AuNRs solution at the juncture of the plates, the pressure differential created due to capillary forces pervades the solution from the bulk drop to the dry zone by forming a thin film. When the water evaporation begins, the AuNRs preferentially form close-packed arrays. At the same time, the vertical substrate's moving velocity is constantly maintained to get controlled arrays. In this technique, all other factors of (a) moving rates of the vertical plate, (b) water evaporation speed, and (c) sample solution concentration can affect the density and thickness of the array. With increasing the glass-plate moving velocity, the density and thickness of the resulting array decrease. The evaporation speed could be modified by controlling the distance between the substrate and a hot wind blower. Increasing the evaporation speed causes the thicknesses of the array to increase.

For this study, about 20 nm × 49 nm sized AuNRs (aperture ratio ∼2.5) were used to create the substrate arrays. The arrays were imaged using FE-SEM. Initially, the difference in affinity of AuNRs toward treated substrates and untreated glass were compared as shown in Figure 3. From the images it is clear that the MPTMS coated surface formed high density AuNR arrays of $1306 \pm 13/\mu m^2$ compared to untreated glass slides with lower AuNRs density of only $458 \pm 7/\mu m^2$. This could be due to the covalent linking between MPTMS and AuNRs. Specifically, strong affinity between the mercapto group of the MPTMS and the gold from AuNRs resulted in an Au−S chemisorption bonding which tethered to the silicon surface of the substrate.[37] The high affinity of the AuNRs toward the MPTMS layer on the substrate produces strongly packed arrays. Even ultrasonication could not break the sulfur−gold bonding (data not shown); thus, the intact array is maintained.

Further, we developed three different densities of AuNR arrays by changing the AuNRs concentrations from 10 to 33 mg/mL. The speed of the moving substrate and the evaporation rate were kept constant throughout the arraying process. Figure 4a,a′ indicates the formation of monolayer arrays at lower concentration of AuNRs solution. The magnified image of Figure 4a′ shows the uniformly distributed AuNRs of 617 ± 9 μm^2 with equal void spaces which shows that the experimental setup was maintained consistently throughout the process; that is, 20 μm/s moving velocity of

15080

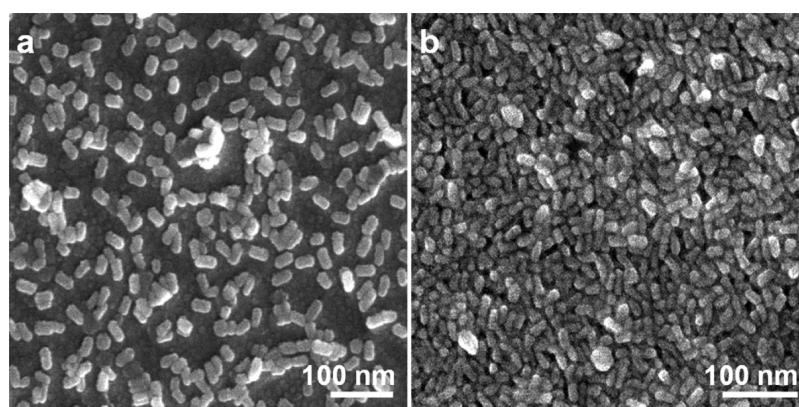dx.doi.org/10.1021/am503153v | ACS Appl. Mater. Interfaces 2014, 6, 15078−15085

Figure 3. FE-SEM images of AuNR arrays on (a) the bare glass substrate with loose nanorod arrangement and (b) MPTMS coated glass substrate showing bushy nanorod arrangement.
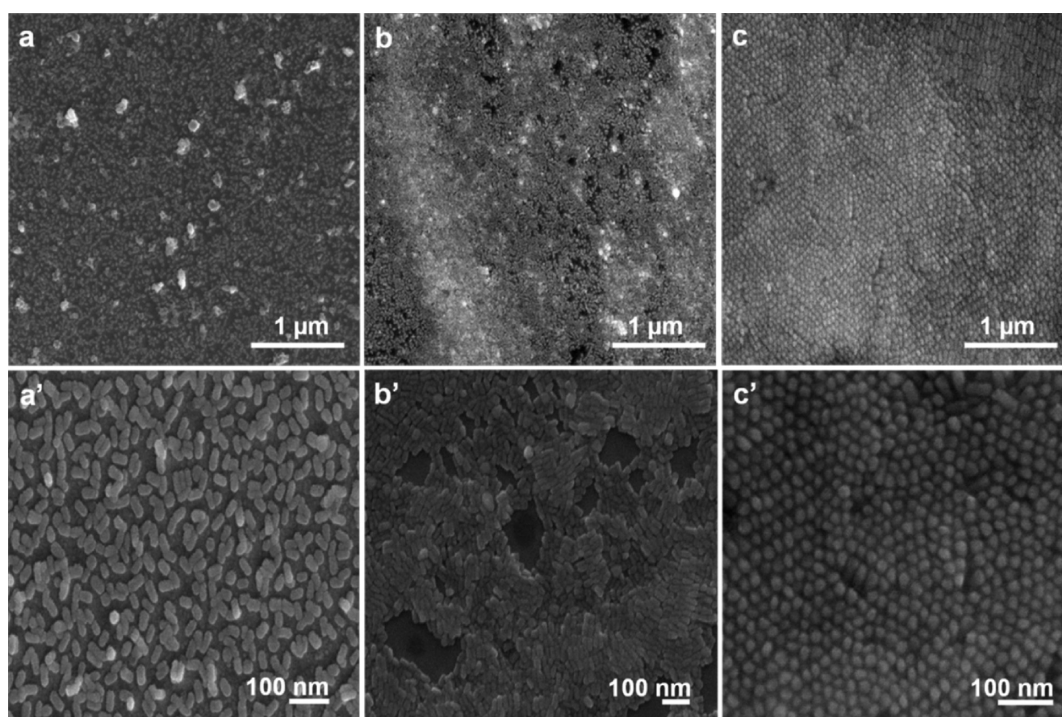

Figure 4. FE-SEM images of convectively assembled AuNR arrays using AuNRs solution concentrations of (a and a′) 10 mg/mL, (b and b′) 20 mg/mL, and (c and c′) 33 mg/mL. (a−c) Low-resolution images; (a′−c′) high-resolution images. With 10 and 20 mg/mL concentrations, two-dimensional (2D) arrays were formed, while for 33 mg/mL, three-dimensional arrays were formed with vertical rod orientation.

the substrate, and the space between glass and hot air blower was maintained at 50 cm. For 20 mg/mL concentration, a monolayer to multilayer with minimum void spaces of AuNR arrays of 1204 ± 12 μm^2 were found in Figure 4b,b′. The void spaces in between nanorods are reduced and the areas of AuNRs coverage have been increased as compared to the previous concentration. The magnified images clearly show the closely packed, horizontally distributed 2D orientation of unorganized AuNR arrays without void space shown in Figure 4b′. This might be achieved due to the convective array technique. A high density array was observed in Figure 4c,c′ using a concentration of 33 mg/mL of AuNRs. With multilayered arrays, very few or no vacant spaces were seen microscopically at this concentration. Figure 4c′ depicts the enlarged view with no empty spaces but closely packed AuNRs of 2092 ± 14 μm^2. Apart from horizontal attachment, most of the AuNRs were aligned in a 3D vertical orientation which can

enhance the surface-plasmon coupling and cause interference to nearby AuNRs when exposed to light.[31] This could be due to the higher concentration of AuNRs. It might also depend on the moving velocity of the substrate and distance to the evaporation hot source in this convective array technique.

Our investigation on AuNR arrays by using convective array techniques shows the linear relationship between concentration of AuNRs solutions, densities of the array formed and the alignment of AuNRs; the higher the concentration, the denser the array formation observed. The small nanoparticles (<100 nm in diameter) were applied with quick fabrication times and accelerated evaporation rates to form 3D structures of arrays by confined convective assembly. Large numbers of substrates can be arrayed with no restrictions on the size of the substrates. The as prepared substrates were utilized to analyze the photothermal lysis behavior on pathogenic bacteria.

3.4. Photothermal Measurements of AuNR Arrays. The AuNR arrays were aimed to lyse pathogenic bacteria, as metal nanoparticles have photothermal energy conversion efficiency. The photothermal response at 200 mW laser energy of the three different concentrations of AuNR arrays are depicted in Figure 5. The photothermal heat production was
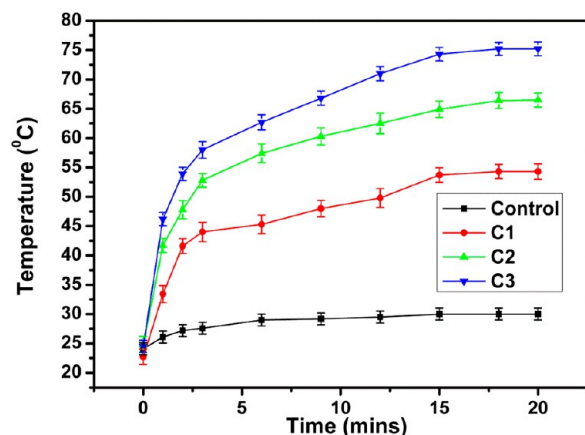

Figure 5. Temperature−time dependent curve of laser irradiated AuNR arrays with different concentrations. C1, C2, and C3 represent concentrations of 10, 20, and 33 mg/mL respectively.

measured on the basis of the method explained by An et al.[38] The radiative properties of the AuNRs and their efficiency to convert light into heat were measured by placing a thermocouple in the vertical direction, that is, in the direction of laser beam propagation. We speculate that the produced heat by laser exposure was initially dissipated in the radial direction; with continued irradiation, the heat penetrated in the axial direction of the array. Compared to reported methods, the AuNR arrays in this study were placed at the bottom of the tube resulting in uniform heat production and constant, isotropic heat transfer to the surrounding medium in all directions, not generally achieved in a system of buoyant nanoparticles. For 10 and 20 mg/mL samples, the maximum temperature measured was 55 and 66 °C, respectively. While for the highest concentration, the maximum temperature attained was more than 75 °C. Initially, after laser illumination on the arrayed substrate the temperature started raising from room temperature and immediately reached to 33.4, 41.7, and 46.2 °C for respective increasing concentrations. After particular time there was no further rise in the maximum temperature reached and that was noted as level-off temperature. Hence, cessation in temperature was observed after this level-off temperature, but the maximum temperature was maintained at a steady state level for long time. The relationship between increasing concentration of AuNRs and raise in temperature was well correlated in this study. From the quantitative results, it was shown that among other concentrations, 33 mg/mL produced substantial temperature increase which could be enough to destroy the pathogenic bacteria. It is proved here that AuNRs are the most promising candidates for photothermal effect since they are the strongest absorbers of light which could convert into heat due to their specific surface plasmon resonance. Especially, 96% of the photons from the light source are absorbed by AuNRs and converted into heat by nonradiative processes.[39] The gold crystal lattice is heated via electron−phonon interaction and cooled by transferring its heat to the surrounding medium via

phonon−phonon relaxation in a picosecond time scale.[40−42] As reported previously, when the maximum absorption of AuNRs' energy shift to near-infrared range, the light energy is converted into more heat energy which could cause irreversible damage to the biological membranes.[43]

The viability of *E. coli* on AuNR array with laser exposure was analyzed using live/dead staining techniques. The assay kit containing SYTO9 and propodium iodide was used to compare and quantify the photothermally lysed bacteria to alive bacteria with the help of fluorescence microscopy images. The SYTO9 enters through the membrane of the bacteria and stains in green color for living bacteria, whereas the propodium iodide gives red color to the lysed bacteria due to the damaged cell wall membrane caused by photothermal lysis. Representative fluorescence microscopy images shown in Figure 6a-d clearly
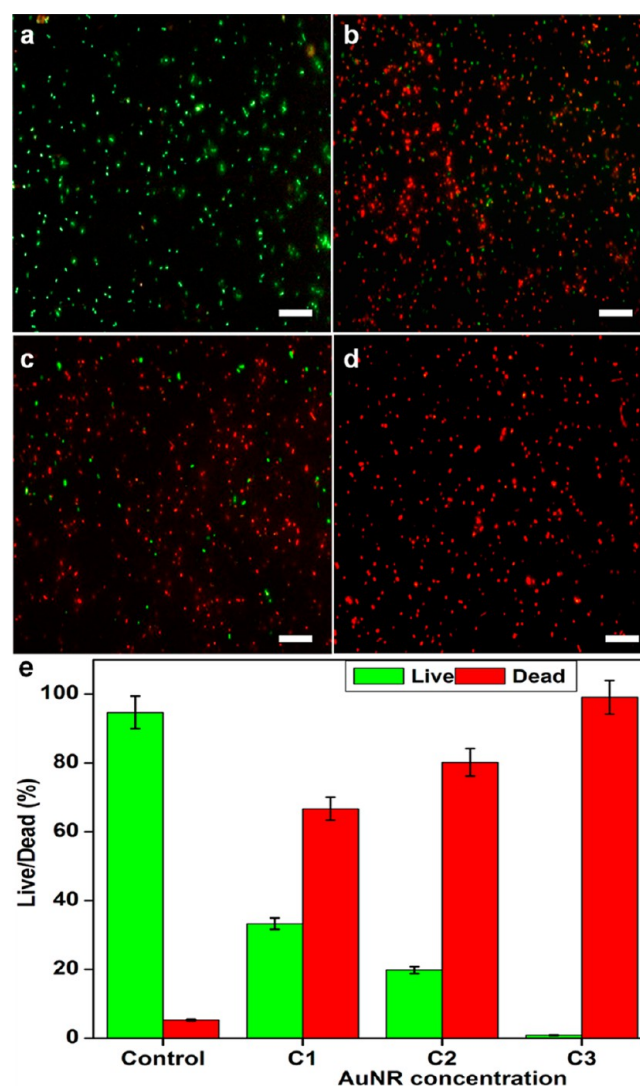

Figure 6. (a−d) Fluorescence microscopy images of *E. coli* cells (a) with only NIR exposure for control, (b) exposed to NIR with 10 mg/mL AuNR arrays, (c) irradiated at NIR with 20 mg/mL AuNR arrays, (d) with NIR irradiation and 33 mg/mL AuNR arrays. Bacteria cells are stained with SYTO9 and PI. Cells with green fluorescent stand for live bacteria, while the red fluorescent cells are representative of dead bacteria. Scale bar equals 10 μm. (e) Histogram of quantitative bacteria survival rate with concentration increase. C1, C2 and C3 represent 10, 20, and 33 mg/mL AuNR arrays, respectively.
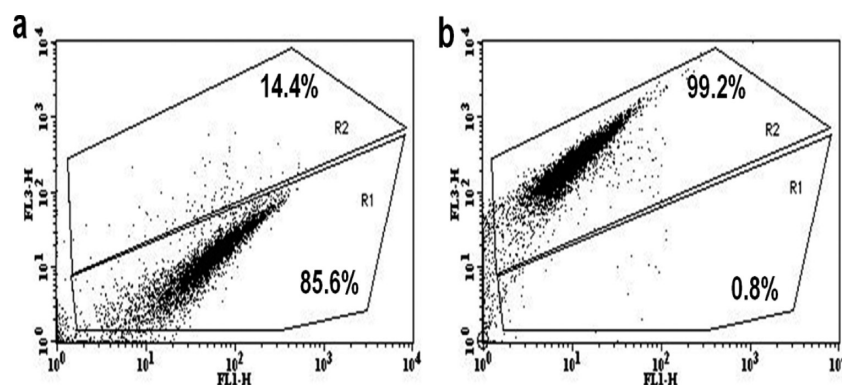
Figure 7. Flow cytometer dot plot of *E. coli* cells (a) only with laser exposure and (b) with laser irradiation and AuNR arrays. Horizontal axis represents SYTO9 fluorescence intensity, while vertical axis stands for PI fluorescence intensity. To determinate the live and dead cells, regions are indicated with R1 for live cells and R2 for dead ones. Percentages of each region are also indicated.

demonstrate the *E. coli* viability/mortality rates. The bacterial lysis is depicted quantitatively in Figure 6e. In a control experiment (without AuNRs), the laser illumination alone did not produce any significant bacterial lysis; thus, the laser impact is negligible.[44] But the increasing AuNRs concentration arrays with laser exposure show corresponding high mortality rates. In total of 15 min, the highest mortality rate of 98% was achieved with the highest concentration of AuNRs (33 mg/mL). On the other hand, 10 and 20 mg/mL concentrations ended only with 68% and 80% lysis, respectively. From the fluorescence microscopy images, it was clearly seen that the concentrations of 10 and 20 mg/mL leave more viable bacteria, that is, considerably more pathogenicity as compared to the 33 mg/mL concentration arrayed substrate which holds less or no pathogenicity. The lethal impact of AuNRs-laser combined photothermal effect could cause blebbing and vesiculation on bacteria with substantial cell destruction. Altogether, our newly developed AuNR array by confined convective arraying technique with laser illumination achieved superior bactericidal activity in a quick succession of time.

As reported by Neumann et al., sustained nanoparticle laser illumination induced the formation of a nanoparticle–bubble complex, which resulted in steam generation and raising the temperature of the fluid medium.[45] Their report strongly supports our hypothesis: the light induced photothermal response of the AuNR arrays caused complete antibacterial sterilization of the samples via the denaturing of the bacterial cells. Our method, however, is totally different and carries certain advantages compared to theirs. For example, it is more convenient in sample handling and can be used to sterilize a particular number of samples in a quick succession of time. In addition, once irradiated, AuNR arrays could be reused for multiple photothermal cycles without loss. More importantly, tailoring the specific wavelength of laser light used to a specific nanoparticle shape further enhances the photon–phonon conversion response. So, in our method, the AuNRs were made to specific dimensions to achieve enhanced photothermal response toward the particular wavelength of laser light used. Altogether, light induced temperature increment of up to 80 °C in the presence of nanoparticles is a quick, efficient, and more adequate method to achieve antibacterial activity compared to the elaborate high temperature sterilization procedures currently employed.

In addition, the flow cytometry analysis was performed against control and laser treated bacteria with the results shown in Figure 7. The figure depicts the unique fluorescence pattern for SYTO9/propodium iodide (PI) dual staining which directly relates to the degree of bacterial mortality. Comparing the *E. coli* viability for the control and the AuNR array treatment, we found that the cell population moved from the low red and strong green fluorescence intensity region (R1) to weak green and heavy red fluorescence intensity region (R2), respectively. The increase of red fluorescence intensity indicated that more PI entered the cells and at the same time quenched the fluorescence intensity of SYTO9.[46,47] For the controlled bacteria sample, almost 90% of bacteria fall in the R1, whereas only 0.8% of AuNRs-NIR treated bacteria did so. Hence, we can see a significant reduction in live bacteria after photothermal exposure for 33 mg/mL AuNR array compared to control. Illustrative dot plots of *E. coli* lysis suggest that AuNRs concentration-dependent membrane damage was produced by the photothermal effect. Hence, it provided more powerful evidence that the bacterial membrane was destroyed, and thus, the bacteria were dead.

The differences in temperature increasing patterns of the photothermal and hot-plate method as a function of time were compared and described in the Figure S1a in the Supporting Information. In the photothermal method, there was an immediate temperature increase up to 50 °C in 1 min by AuNR arrays. In contrast, at the same interval of time of 1 min, the hot-plate method showed slow, steady state temperature rise from room temperature to about 28.3 °C. In the hot-plate method, the temperature reached more than 91.2 °C in 20 min. There was a continuous thermal loss from the heat source to the surrounding due to heat dissipation which led to more time consumption for reaching the required maximum temperature. Autoclaving could be recommended for complete sterilization, but it requires the investment of more energy and time. Our study indicates that better-controlled higher temperatures can be obtained in shorter times in an optimized photothermal method compared to sterilization methods.

Figure S1b in the Supporting Information depicts our quantitative analysis of the difference in bacterial mortality rate of pathogenic *E. coli* between the photothermal and hot-plate methods. The control sample showed a negligibly small number of dead bacteria. The hot-plate method reached about 91.2 °C in 20 min and ended with 90% bacteria lyses. The photothermal method attained about 75.2 °C at the same time interval of 20 min and achieved almost 100% pathogen destruction. So, compared to the hot-plate method, our AuNR

array based photothermal method resulted in superior pathogen lyses. Most importantly, the hot-plate method failed to destroy the pathogenic bacteria completely, leaving the suspension possessing some degree of pathogenicity after treatment. Altogether, the photothermal method of our AuNR arrays in the presence of laser irradiation achieved superior antibacterial activity with 100% cell destruction as compared to the conventional, large energy, and more time-consuming hot-plate methods.

4. CONCLUSION

In summary, when the nanorod concentration was controlled, 2D or 3D AuNR arrays were formed in a quick succession of time using confined convective assembly methods and further characterized by FE-SEM. The antibacterial properties of AuNR arrays toward *E. coli* were studied by using laser illumination on the nanorod arrayed substrate. Fluorescence microscopy, Bio-AFM and flow cytometry were utilized to measure the bacterial viability. With the highest concentration of AuNR arrays upon laser illumination, 98% of the *E. coli* was photothermally destroyed causing irreparable cellular damage, which demonstrated that our arrays were highly effective in killing bacteria. The results indicated that the combined photothermal treatment using AuNR arrays and NIR laser light can be applicable as a highly efficient, direct, rapid, and real time destruction of pathogenic bacteria. Therefore, we believe AuNR arrays have a promising prospect in the photothermal eradication of pathogenic bacteria from water. Although this is our initial attempt to control pathogenic bacterial population in a stable water system by photothermal techniques, further optimization is required in order to apply AuNR arrays to purify flowing drinking water by mimicking water purification devices. Most, importantly, the AuNR arrays are efficient and reusable due to their quick photothermal energy conversion, well-defined temperature increasing rate, and ease of handling from one sample to another.

■ ASSOCIATED CONTENT

ⓢ Supporting Information

Additional experimental data collected on fluid temperature increase as a function of time and histograms of quantitative bacterial survival rate analysis for both the photothermal and the hot-plate methods. This material is available free of charge via the Internet at http://pubs.acs.org.

■ AUTHOR INFORMATION

Corresponding Author
*E-mail: vitalis@mju.ac.kr.

Author Contributions
‖These authors contributed equally to this work.

Notes
The authors declare no competing financial interest.

■ ACKNOWLEDGMENTS

■ REFERENCES

(1) Swaminathan, B.; Barrett, T. J.; Hunter, S. B.; Tauxe, R. V. CDC PulseNet Task Force'. PulseNet: The Molecular Subtyping Network for Foodborne Bacterial Disease Surveillance, United States. *Emerging Infect. Dis.* **2001**, *7*, 382−389.

(2) Li, X. J.; Kolltveit, K. M.; Tronstad, L.; Olsen, I. Systemic Diseases Caused by Oral Infection. *Clin. Microbiol. Rev.* **2000**, *13*, 547−558.

(3) Mead, P. S.; Slutsker, L.; Dietz, V.; McCaig, L. F.; Bresee, J. S.; Shapiro, C.; Griffin, P. M.; Tauxe, R. V. Food-Related Illness and Death in the United States. *Emerging Infect. Dis.* **1999**, *5*, 607−625.

(4) Etsuzo, E.; Mito, A.; Shigetomo, T.; Yoshinori, T.; Michio, O. Antibacterial Action of Vinegar against Food-Borne Pathogenic Bacteria Including *Escherichia coli* O157:H7. *J. Food Prot.* **1998**, *8*, 929−1086.

(5) Demerec, M. Origin of Bacterial Resistance to Antibiotics. *J. Bacteriol.* **1948**, *56*, 63−74.

(6) Okeke, I. N.; Lamikanra, A.; Edelman, R. Socioeconomic and Behavioral Factors Leading to Acquired Bacterial Resistance to Antibiotics in Developing Countries. *Emerging Infect. Dis.* **1999**, *5*, 18−27.

(7) Hyland, R. M.; Beck, P.; Mulvey, G. L.; Kitov, P. I.; Armstrong, G. D. N-Acetyllactosamine Conjugated to Gold Nanoparticles Inhibits Enteropathogenic *Escherichia coli* Colonization of the Epithelium in Human Intestinal Biopsy Specimens. *Infect. Immun.* **2006**, *74*, 5419−5421.

(8) Letfullin, R. R.; Joenathan, C.; George, T. F.; Zharov, V. P. Laser-Induced Explosion of Gold Nanoparticles: Potential Role for Nanophotothermolysis of Cancer. *Nanomedicine* **2006**, *1*, 473−480.

(9) Morones, J. R.; Elechiguerra, J. L.; Camacho, A.; Holt, K.; Kouri, J. B.; Ramirez, J. T.; Yacaman, M. J. The Bactericidal Effect of Silver Nanoparticles. *Nanotechnology* **2005**, *16*, 2346−2353.

(10) Xu, L.; Liu, Y.; Chen, Z.; Li, W.; Liu, Y.; Wang, L.; Liu, Y.; Wu, X.; Ji, Y.; Zhao, Y.; Ma, L.; Shao, Y.; Chen, C. Surface-Engineered Gold Nanorods: Promising DNA Vaccine Adjuvant for HIV-1 Treatment. *Nano Lett.* **2012**, *12*, 2003−2012.

(11) Cheng, F. Y.; Chen, C. T.; Yeh, C. S. Comparative Efficiencies of Photothermal Destruction of Malignant Cells Using Antibody-Coated Silica@Au Nanoshells, Hollow Au/Ag Nanospheres and Au Nanorods. *Nanotechnology* **2009**, *20*, 425104.

(12) Truong, P. L.; Kim, B. W.; Sim, S. J. Rational Aspect Ratio and Suitable Antibody Coverage of Gold Nanorod for Ultra-Sensitive Detection of a Cancer Biomarker. *Lab Chip* **2012**, *12*, 1102−1109.

(13) Yang, S. H.; Ye, F.; Xing, D. Intracellular Label-Free Gold Nanorods Imaging with Photoacoustic Microscopy. *Opt. Express* **2012**, *20*, 10370−10375.

(14) Gou, L. F.; Murphy, C. J. Fine-Tuning the Shape of Gold nanorods. *Chem. Mater.* **2005**, *17*, 3668−3672.

(15) Kim, C. B.; Yi, D. K.; Kim, P. S.; Lee, W.; Kim, M. J. Rapid Photothermal Lysis of the Pathogenic Bacteria, *Escherichia coli* Using Synthesis of Gold Nanorods. *J. Nanosci. Nanotechnol.* **2009**, *9*, 2841−2845.

(16) Petrova, H.; Hu, M.; Hartland, G. V. Photothermal Properties of Gold Nanoparticles. *Z. Phys. Chem.* **2007**, *221*, 361−76.

(17) Choi, W. I.; Sahu, A.; Kim, Y. H.; Tae, G. Photothermal Cancer Therapy and Imaging Based on Gold Nanorods. *Ann. Biomed. Eng.* **2011**, *40*, 534−546.

(18) Harris, N.; Ford, M. J.; Mulvaney, P.; Cortie, M. B. Tunable Infrared Absorption by Metal Nanoparticles: the Case for Gold Rods and Shells. *Gold Bull.* **2008**, *41*, 5−14.

(19) Leea, H. J.; Yasukawab, T.; Suzukia, M.; Leec, S. H.; Yaoc, T.; Takid, Y.; Tanakad, A.; Kameyamad, M.; Shikua, H.; Matsue, T. Simple and Rapid Preparation of Vertically Aligned Gold Nanoparticle Arrays and Fused Nanorods in Pores of Alumina Membrane Based on Positive Dielectrophoresis. *Sens. Actuators, B* **2008**, *136*, 320−325.

(20) Moon, J. M.; Wei, A. Uniform Gold Nanorod Arrays from Polyethylenimine-Coated Alumina Templates. *J. Phys. Chem. B* **2005**, *109*, 23338−23341.

(21) Sau, T. K.; Murphy, C. J. Self-Assembly Patterns Formed upon Solvent Evaporation of Aqueous Cetyltrimethylammonium Bromide-Coated Gold Nanoparticles of Various Shapes. *Langmuir* **2005**, *21*, 2923−2929.

(22) Kim, F.; Kwan, S.; Akana, J.; Yang, P. Langmuir-Blodgett Nanorod Assembly. *J. Am. Chem. Soc.* **2001**, *123*, 4360−4361.

(23) Paviolo, C.; Haycock, J. W.; Yong, J.; Yu, A.; Stoddart, P. R.; McArthu, S. L. Laser Exposure of Gold Nanorods Can Increase Neuronal Cell Outgrowth. *Biotechnol. Bioeng.* **2013**, *110*, 2277−2291.

(24) Jo, W.; Lee, J. H.; Kim, M. J. Temperature Measurement in A Single Patterned Gold Nanorod Cluster Using Laser-Induced Fluorescence. *J. Nanopart. Res.* **2012**, *14*, 699.

(25) Tong, L.; Wei, Q.; Wei, A.; Cheng, J. X. Gold Nanorods as Contrast Agents for Biological Imaging: Optical Properties, Surface Conjugation and Photothermal Effects. *Photochem. Photobiol.* **2009**, *85*, 21−32.

(26) Letfullin, R. R.; Joenathan, C.; George, T. F.; Zharov, V. P. Laser-Induced Explosion of Gold Nanoparticles: Potential Role for Nanophotothermolysis of Cancer. *Nanomedicine* **2006**, *1*, 473−480.

(27) Nikoobakht, B.; El-Sayed, M. A. Preparation and Growth Mechanism of Gold nanorods (NRs) Using Seed-Mediated Growth Method. *Chem. Mater.* **2003**, *15*, 1957−1962.

(28) Sau, T. K.; Murphy, C. J. Seeded High Yield Synthesis of Short Au Nanorods in Aqueous Solution. *Langmuir* **2004**, *20*, 6414−6420.

(29) Seguin, C.; McLachlan, J. M.; Norton, P. R.; Lagugne -Labarthet, F. Surface Modification of Poly(dimethylsiloxane) for Microfluidic Assay Applications. *Appl. Surf. Sci.* **2010**, *256*, 2524−2531.

(30) Dimitrov, A. S.; Nagayama, K. Continuous Convective Assembling of Fine Particles into Two-Dimensional Arrays on Solid Surfaces. *Langmuir* **1996**, *12*, 1303−1311.

(31) Yi, D. K.; Lee, J. H.; Rogers, J. A.; Paik, U. Two-Dimensional Nanohybridization of Gold Nanorods and Polystyrene Colloids. *Appl. Phys. Lett.* **2009**, *94*, 084104.

(32) Schottner, G. Hybrid Sol-Gel-Derived Polymers: Applications of Multifunctional Materials. *Chem. Mater.* **2001**, *13*, 3422−3435.

(33) Seguin, C.; McLachlan, J. M.; Norton, P. R.; Lagugne-Labarthet, F. Surface Modification of Poly(dimethylsiloxane) for Microfluidic Assay Applications. *Appl. Surf. Sci.* **2010**, *256*, 2524−2531.

(34) Flinn, D. H.; Guzonas, D. A.; Yoon, R. H. Characterization of Silica Surfaces Hydrophobized by Octadecyltrichlorosilane. *Colloids Surf., A* **1994**, *87*, 163−176.

(35) Chen, J. J.; Struk, K. N.; Brennan, A. B. Surface Modification of Silicate Glass Using 3-(Mercaptopropyl)trimethoxysilane for Thiol−Ene Polymerization. *Langmuir* **2011**, *27*, 13754−13761.

(36) Ormonde, A. D.; Hicks, E. C.; Castillo, J.; VanDuyne, R. P. Nanosphere Lithography: Fabrication of Large-Area Ag Nanoparticle Arrays by Convective Self-Assembly and Their Characterization by Scanning UV-Visible Extinction Spectroscopy. *Langmuir* **2004**, *20*, 6927−6931.

(37) Khatri, O. P.; Adachi, K.; Murase, K.; Okazaki, K. I.; Torimoto, T.; Tanaka, N.; Sugimura, H. Self-Assembly of Ionic Liquid (BMI-PF6)-Stabilized Gold Nanoparticles on A Silicon Surface: Chemical and Structural Aspects. *Langmuir* **2008**, *24*, 7785−7792.

(38) An, W.; Zhu, Q.; Zhu, T.; Gao, N. Radiative Properties of Gold Nanorod Solutions and Its Temperature Distribution under Laser Irradiation: Experimental Investigation. *Exp. Therm. Fluid Sci.* **2013**, *44*, 409−418.

(39) Link, S.; El-Sayed, M. A. Shape and Size Dependence of Radiative, Non-Radiative and Photothermal Properties of Gold Nanocrystals. *Int. Rev. Phys. Chem.* **2000**, *19*, 409−453.

(40) Huang, X.; Jain, P. K.; El-Sayed, I. H.; El-Sayed, M. A. Plasmonic Photothermal Therapy (PPTT) Using Gold Nanoparticles. *Cancer Lett.* **2008**, *23*, 217−228.

(41) El-Sayed, M. A. Some Interesting Properties of Metals Confined in Time and Nanometer Space of Different Shapes. *Acc. Chem. Res.* **2001**, *34*, 257−264.

(42) Yi, D. K. A Study of Optothermal and Cytotoxic Properties of Silica Coated Au Nanorods. *Mater. Lett.* **2011**, *65*, 2319−2321.

(43) Ramasamy, M.; Lee, S. S.; Yi, D. K.; Kim, K. Magnetic, Optical Gold Nanorods for Recyclable Photothermal Ablation of Bacteria. *J. Mater. Chem. B* **2014**, *2*, 981−988.

(44) Wu, M. C.; Deokar, A. R.; Liao, J. H.; Shih, P. Y.; Ling, Y. C. Graphene-Based Photothermal Agent for Rapid and Effective Killing of Bacteria. *ACS Nano* **2013**, *7*, 1281−1290.

(45) Neumann, O.; Feronti, C.; Neumann, A. D.; Dong, A.; Schelld, K.; Lu, B.; Kim, E.; Quinn, M.; Thompson, S.; Grady, N.; Nordlandera, P.; Oden, M.; Halas, N. J. Compact Solar Autoclave Based on Steam Generation Using Broadband Light-Harvesting Nanoparticles. *Proc. Natl. Acad. Sci. U.S.A.* **2013**, *110*, 11677−81.

(46) Berney, M.; Hammes, F.; Bosshard, F.; Weilenmann, H. U.; Egli, T. Assessment and Interpretation of Bacterial Viability by Using the LIVE/DEAD BacLight Kit in Combination with Flow Cytometry. *Appl. Environ. Microbiol.* **2007**, *73*, 3283−3290.

(47) Berney, M.; Weilenmann, H. U.; Egli, T. Flow-Cytometric Study of Vital Cellular Functions in *Escherichia Coli* During Solar Disinfection (SODIS). *Microbiology* **2006**, *152*, 1719−1729.